Zeszyty Naukowe Wydziału
Elektroniki i Informatyki
Politechniki Koszalińskiej

ISSN:1897-7421
Nr 15, 2019
Str: 35-56

B. Andriyevsky [1]
A. Kashuba [2]
H. Ilchuk [2]
[1]Faculty of Electronics and Computer Sciences
Koszalin University of Technology,
Śniadeckich str. 2, PL-75-453, Koszalin, Poland
[2]Lviv Polytechnic National University,
Bandera str. 12, 79646 Lviv, Ukraine
bohdan.andriyevskyy@tu.koszalin.pl

Effect of crystal defects on the electronic structure and dielectric functions of $In_{0.5}Tl_{0.5}I$ solid state solutions

Keywords: semiconductors, point defects, electronic band structure, electrical transport, optical properties, computer simulations

1. Introduction

Searching the new functional materials with tunable physical properties is of key interest for current micro and optoelectronics. Over the past few decades the attention of scientists is being focused on the searching new materials with possibilities the controlled tuning of the physical properties. In particular, modifications of initial material for achieve the expected properties suitable for potential applications can be performed in many ways. One of the popular and effective methods is a gradual substitution one of the components by another belonging to the same group of the periodic system of elements. Such a procedure introduces internal stress into the already known crystals (mostly caused by mismatch of ionic radiuses) and creates solid solutions based on a pristine crystal [1, 2]. So far, we have successfully tuned properties of several crystals by changing composition and utilizing structure-properties relations for such modified compounds, using both experimental methods and computer simulations [3 - 5].

As well known, during crystal growth processes, all kinds of defects always appear: twinning's, interstitials, vacancies or atomic positions exchange [6].

Structural defects substantially affect the electronic structure of a material, cause changes of the optical properties, transport phenomena and finally influence its structural stability. In many cases, the controlled level of certain defects may positively influence the expected properties of materials, improving desired features such as non-linear optical, thermoelectric, etc. Often, significant differences between the experimentally measured and computationally simulated data are caused by not only the limitations of the applied theoretical models or computational techniques (e.g. the well-known underestimation of the band gap obtained with using the density functional theory) but because of the disregard the ubiquitous defects existing in real crystals. In the present study, the influence of crystal structure deviations of the ternary crystals $In_xTl_{1-x}I$ and its solid solution from the perfect one on the corresponding electron related properties was computationally investigated by using the density functional theory (DFT) approach. Comparison of the computational results obtained in the present investigation with our previous experimental and theoretical studies of the same materials confirms the effectiveness of the structure defects models adopted. The method proposed in this work can be extended to modeling and prediction the properties of new crystalline materials or to verify compliance the previous calculations made with the assumption of a perfect structure and corresponding experimental data.

2. Materials: $In_xTl_{1-x}I$

Thallium, embedded in a stable crystal matrix, having saturated bonds, is not as dangerous as a free atom or ion, while the chemical compounds that contain it possess extremely interesting optical properties [3,4] and are excellent thermoelectric materials [7]. Among the mixed semiconductors of the $A^{III}V^{VII}$ group the three-component crystals $In_xTl_{1-x}I$, representing a continuous series of solid solutions of substitution (SSS), may be promising for applications in optoelectronics in spite of investigations these SSSs many years ago [8 - 10]. Their band gap E_g vary within the range 2.01 - 2.84 eV [8 - 11]. The crystals possess a layered structure. However, in contrast to typical layered crystals of the $A^{II}B^{VII}$ and $A^{III}B^{VI}$ (CdI_2, HgI_2, GaSe, InSe) groups [12, 13], in which the van der Waals interlayer gaps are formed mainly by the corresponding anions, in $In_xTl_{1-x}I$ SSS, this weakest chemical bonding is probably created by indium and thallium cations and iodine anions. Investigations of the crystals $In_xTl_{1-x}I$ is of interest due to the possibility of samples growth combining the properties of both InI and TlI. The application prospect of these compounds is associated with their use as materials in the ionizing radiation detectors and optical modulators of CO_2 laser [14]. The crystal structure of TlI was firstly investigated at ambient temperature [15]: Z = 4, orthorhombic, space group *Cmcm*, $a = 4.57$, $b = 12.92$, $c = 5.24$ Å. In turn, the crystal structure of InI has been determined in works [16, 17]: InI, structure type TlI, Z = 4, orthorhombic,

space group No. 63 (*Cmcm*), $a = 4.763$, $b = 12.781$, $c = 4.909$ Å. The space group of symmetry for InI crystal is the same as for TlI one.

Thallium iodide crystallizes in a rhombic structure at the temperatures up to 178 °C, but at higher temperatures, it transforms into the CsCl structure of the cubic symmetry. Information on the corresponding structural phase transition is presented in work [18]. In halides of indium, no phase transitions occur except in InCl. The crystals InI and TlI cleave perpendicularly to the crystallographic *b*-axis [8 - 13]. Smooth controlled changes of the energy band gap E_g, mechanical and photovoltaic characteristics and spectral range of the recombination radiation may be realized in them. Results of investigation of the band structure and photoconductivity with change of the indium vs thallium content of the crystals $In_xTl_{1-x}I$ are presented in the recent study [11].

So far, studies of the phonon spectra, mechanical and optical characteristics are known for $In_xTl_{1-x}I$ SSS [19 - 22]. In Ref. [19], a possibility of forming the InI structure as a matrix for the TlI quantum dots inclusion is discussed. The reduction of the crystal unit cell dimensions *b* and *c* and the unit cell volume *V* and the increase of dimension *a* together with the increase of content index *x* are the main features indicating the continuous structure changes of $In_xTl_{1-x}I$ [11] (in the previous Refs. [8 - 13] and [17 - 22], the convention $a \approx c < b$ for the unit cell dimension was adopted).

The optical anisotropy, which is expected due to the layer structure, and the continuous structure transformations mentioned above make $In_xTl_{1-x}I$ SSS perspective for the nonlinear optics and electrical engineering applications. For this purpose, the details of the phenomena associated with such applications of $In_xTl_{1-x}I$ SSS should be studied. In particular, it was found [11] that the photoconductivity spectra in the *ac* layer of $In_xTl_{1-x}I$ SSS correspond to the *n*- and *p*-types carriers. It was also suggested that the appearance of the *n*-type conductivity, occurred primarily in the *a*- crystallographic direction of $In_xTl_{1-x}I$, is caused by the anionic vacancy or cationic interstitials. If an alternation of the conductive and insulating sub-layers along the *b* unit cell dimension of the crystal is possible, one can assume that $In_xTl_{1-x}I$ SSS may be used as a material for the low-dimensional capacitors. From this point of view, one of the main goals of this work is to study the origin of electric conductivity and the quasi-metallization of $In_xTl_{1-x}I$ SSS.

If the suggested anionic vacancies or cationic interstitials in $In_xTl_{1-x}I$ SSS lead to the quasi-metallization, this should be revealed in the band structure and dielectric function of the material. The present study is based on the first principles calculations in the framework of the density functional theory (DFT) of the band structure (BS) and dielectric functions of the nominally pure crystal $In_{0.5}Tl_{0.5}I$ and on the changes of these characteristics caused by the anionic vacancies and cationic interstitials in the compound.

3. Calculations

Calculations of BS and related properties of the materials were carried out using the academic CASTEP code [23] in the framework of DFT approach. The calculations were performed within the generalized gradient approximation (GGA) with the Perdew-Burke-Ernzerhof (PBESOL) exchange-and-correlation functional [24]. The interaction of electrons with atomic cores was described with the norm-conserving pseudopotentials supplied with the academic CASTEP [23].

The electronic wave functions are expanded in a plane wave basis set with the energy cut-off of 650 eV. The atomic levels $4d^{10}5s^25p^1$ for indium, $5d^{10}6s^26p^1$ for thallium and $5s^25p^5$ for iodine atoms are treated as valence electron states. For the Brillouin zone (BZ) sampling, we have used the Monkhorst–Pack *K*-points meshes [25] of 0.0625 $Å^{-1}$. The self-consistent convergence of the total energy was chosen to be 1.0×10^{-6} eV/atom. For DFT calculations of the non-defective and defective $In_xTl_{1-x}I$ SSS the supercells, representing 2×2×2 unit cells containing 64 atoms, were created. The crystal symmetry of the optimized non-defective $In_xTl_{1-x}I$ SSS at $x = 0.5$ is lower (No. 38, *Amm*2) than the space group of symmetry for InI or TlI crystals (No. 63, *Cmcm*). The geometry optimization of lattice parameters and internal atomic coordinates were determined using the Broyden–Fletcher–Goldfarb–Shanno minimization technique (BFGS) with the maximum ionic Hellmann–Feynman forces within 0.02 eV/Å, the maximum ionic displacement within 1.0×10^{-3} Å, and the maximum stress within 0.05 GPa.

4. Results and discussion

The crystal structure of $In_{0.5}Tl_{0.5}I$ SSS has been obtained by the replacement of two indium atoms by the thallium ones in the conventional unit cell of InI (In_4I_4). For the purpose of the proper BZ sampling of the crystals studied using the 'SeeK-path' tool [26] the sequence of the Cartesian axes and corresponding unit cell dimensions and atomic coordinates has been changed to satisfy the relation $a(X) < b(Y) < c(Z)$, where $a = 4.763$, $b = 4.909$, $c = 12.781$ Å.

Symmetry requirements of $In_{0.5}Tl_{0.5}I$ crystal (space group No. 38) cause that *x*- and *y*-conventional coordinates of each atom remain constant (0.0, 0.25, 0.5 or 0.75) and only the *z*-coordinates of atoms may change during structure optimization together with the unit cell dimensions *a*, *b* and *c*. We have found, however, that the parameter of the unit cell elongation $2c/(a + b)$ of the optimized $In_2Tl_2I_4$ crystal (2.638) is close to the similar values in In_4I_4 (2.645) and Tl_4I_4 (2.638) ones.

We have studied also the defective $In_{0.5}Tl_{0.5}J$ SSSs: with iodine vacancy (1) and with thallium interstitial atom (2). With this aim, the primitive or conventional unit cells, possessing too small crystal cell dimensions, are not convenient. To prevent the direct interaction between neighboring iodine vacancies or thallium interstitials

the supercell 2×2×2 of the conventional unit cell of $In_2Tl_2J_4$ with the dimensions $a = 9.010$ Å, $b = 9.284$ Å and $c = 26.216$ Å, containing 64 atoms ($In_{16}Tl_{16}I_{32}$), has been used for calculations (Figs. 1, 2). Two different localizations of the iodine vacancy I1 and I2 are possible relating to the initial structure $In_{16}Tl_{16}I_{32}$ (Fig. 1). In the first localization I1, the smallest distance I1 - Tl (3.302 Å) is smaller than the smallest distance I1 - in (3.409 Å). In turn, in the second localization I2, the smallest distance I2 - In (3.157 Å) is smaller than the smallest distance I2 - Tl (3.432 Å). To study the defective $In_{0.5}Tl_{0.5}J$ SSS with thallium interstitial atom, we have used the initial structure $In_{16}Tl_{16}I_{32}$, to which one thallium atom has been added into the supercell center corresponding to the most probable localization of large interstitial atom (Fig. 2). Thus, three crystal structures of the defective $In_{0.5}Tl_{0.5}J$ SSS have been studied: two supercells 2×2×2 with one I1 or I2 vacancy and one supercell 2×2×2 with one Tl interstitial. Every of these three defective crystal structures possess the space group of symmetry No. 25 (*Pmm*2).

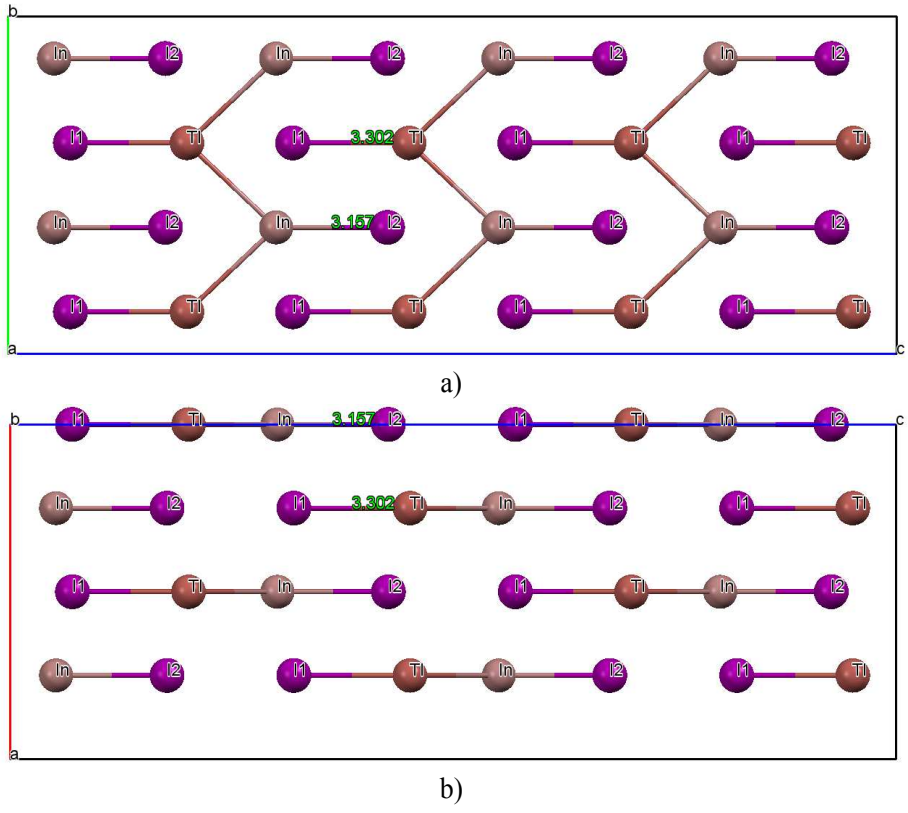

Fig. 1. Views along *a*- (a) and *b*-axis (b) of the optimized structure of $In_{16}Tl_{16}I_{32}$ crystal ($a = 9.527$ Å, $b = 9.575$ Å, $c = 25.193$ Å). Interatomic distances Tl – I1 and In – I2 are presented in Angstrom

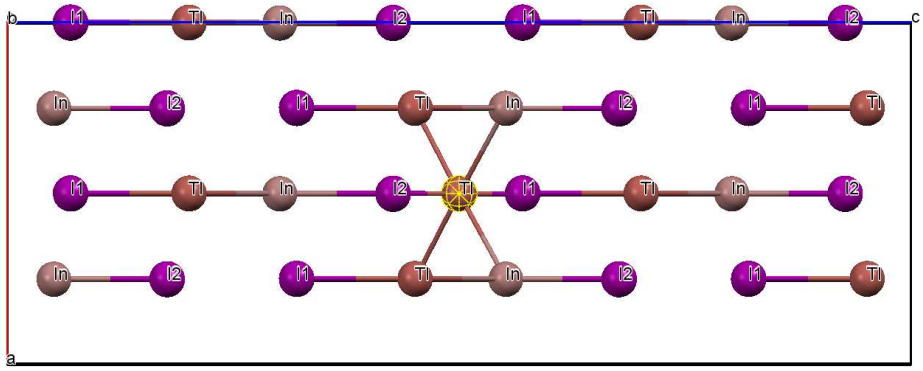

Fig. 2. View along *a*-axis of the initial structure of $In_{16}Tl_{17}I_{32}$ crystal (a = 9.527 Å, b = 9.575 Å, c = 25.193 Å) with one interstitial thallium atom indicated by yellow net

The CASTEP calculations of BS were carried out at the points of Brillouin zone (BZ) determined using the 'SeeK-path' tool [26]. Because of the different space groups of symmetry in the cases of crystals InI (TlI), $In_{0.5}Tl_{0.5}I$ and defective crystals $In_{0.5}Tl_{0.5}I$, the corresponding sets of *K*-points for the BS calculations are different.

For the cases of the primitive unit cells used, the calculated band gap E_g of InI has been found to be indirect. In turn, the direct band gaps E_{gd} have been detected for $In_{0.5}Tl_{0.5}I$ and TlI crystals, which are not located at Γ-point of BZ (Fig. 3). For $In_{0.5}Tl_{0.5}I$ the direct energy band gap E_{gd} takes place at the *K*-point -1/2,1/2,1/3 at the boundary of the first BZ, not at the Γ-point 0,0,0 (Fig. 3). The value of band gap found, E_g = 1.315 eV, may correspond to either direct or indirect electron transitions (Fig. 3). Almost inverse proportional dependence of the band gap $E_g(x)$ on the content parameter x ($In_xTl_{1-x}I$) can be noticed: $E_g(x = 0) = 2.2$ eV, $E_g(x = 0.5) = 1.3$ eV, $E_g(x = 1.0) = 0.61$ eV (see Table 1), what is in agreement with previous results [11]. The calculated values of E_g are smaller than the experimentally observed ones, that occurs often for DFT calculations of crystals. A clear dependence between Hirshfeld charges of ions in InI, $In_{0.5}Tl_{0.5}I$ and TlI crystals and their band gap values is observed (Table 1). In $In_{0.5}Tl_{0.5}I$ SSS, the smallest interatomic distance $d_{In\text{-}I}$ = 3.13 Å is smaller than the corresponding value in InI (3.22 Å), and the smallest distance $d_{Tl\text{-}I}$ = 3.33 Å is larger than the similar one in TlI (3.23 Å). This may be explained using the electronegativity values for indium (1.7), thallium (1.8) and iodine (2.5) atoms [27]. The larger the difference of the electronegativity values of two atoms the larger the ionicity of the corresponding chemical bond. In view of the prevailing ionic bonding in the crystals studied, one may expect larger ion-ion interactions In - I in comparison to Tl - I ones, that may lead to the mentioned changes of equilibrium interatomic distances in $In_{0.5}Tl_{0.5}I$ in comparison to InI and TlI.

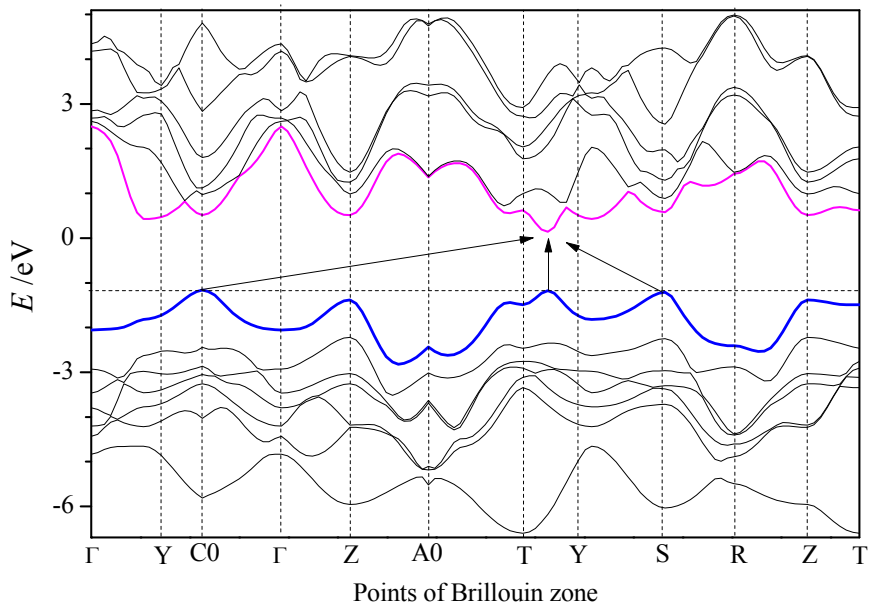

Fig. 3. Band structure of $InTlI_2$ SSS. Top VB and bottom CB are indicated by color lines. Probable transitions corresponding to band gap E_g are shown by arrows. The *K*-points list used, Γ - 0,0,0; Y - -1/2,1/2,0; C0 - -0.286,0.714,0; Γ - 0,0,0; Z – 0,0,1/2; A0 - 0.286,0.286,1/2; T - -1/2,1/2,1/2; Y - -1/2,1/2,0; S – 0,1/2,0; R – 0,1/2,1/2; Z – 0,0.1/2; T - -1/2,1/2,1/2 corresponds to the space group of symmetry No. 38 (*Amm*2)

Table 1. The Hirshfeld charges q and smallest interatomic distances d for InI, $In_{0.5}Tl_{0.5}I$ and TlI crystals calculated at primitive unit cell

Crystal Value	InI	$In_{0.5}Tl_{0.5}I$	TlI
q_{In1} or q_{Tl1} /e	0.11	0.12 (In)	0.14
q_{In2} or q_{Tl2} /e	0.11	0.13 (Tl)	0.14
q_{I1} /e	-0.11	-0.13	-0.14
q_{I2} /e	-0.11	-0.12	-0.14
$d_{In\text{-}I}$ /Å	3.22	3.13	-
$d_{Tl\text{-}I}$ /Å	-	3.33	3.23
E_g /eV	0.61	1.3	2.2

Another characteristic property of the band structure of semiconductors is a tensor of effective electron mass m^*_{ij} [28],

$$\left(m^{*-1}\right)_{ij} = \frac{1}{\hbar^2}\frac{\partial^2 E}{\partial K_i \partial K_j} \tag{1}$$

which is usually presented in terms of the free electron mass m_e. Information on the effective electron mass m^* is important because this parameter determines the dynamics of electron conductivity in material and therefore is significant for the practical applications.

In order to see difference between the effective electron masses in $In_xTl_{1-x}J$ for $x = 0$, 0.5 and 1.0 at the same K-point set corresponding to the space group of symmetry No. 38, the band structure calculations have been performed at the corresponding primitive unit cells. The effective mass tensor m^*_{ij} was calculated using the Effective Mass Calculator code [29] at the bands extrema using finite difference method with the step value of 0.02 (Bohr^{-1}). The calculated diagonal components m^*_{ii} ($i = 1, 2, 3$) of the effective mass tensor m^*_{ij} ($i, j = 1, 2, 3$) are presented in Table 2 and Table 3. There are no clear dependences of effective mass m^* on the content parameter x. However, by more detailed analysis of the Table 2 and Table 3 one may reveal that for the selected components of the effective mass tensor m^*_{ij} a tendency to decrease the absolute values $|m^*_{ii}|$ with increase of the content parameter x can be noticed. More reliable conclusion relating the dependence of the electron effective mass in $In_xTl_{1-x}I$ SSS may be derived from the study of the problem for more values of the content parameter x. This, however, was not among our first aims in this work.

Table 2. Diagonal components m^*_{ii} of the effective mass tensor m^*_{ij} for top VB of $In_xTl_{1-x}I$ crystals, calculated at selected K-points of BZ of primitive unit cells: C0 – -0.285,0.714,0; Z – 0,0,0.5; A0 – 0.285,0.285,0.5; TY - -0.5,0.5,0.2727; S – 0,0.5,0 (see Fig. 3)

VB	$x = 1.0$			$x = 0.50$			$x = 0$		
	m^*_{11}	m^*_{22}	m^*_{33}	m^*_{11}	m^*_{22}	m^*_{33}	m^*_{11}	m^*_{22}	m^*_{33}
C0	-0.070	-0.294	-0.456	-0.043	-0.177	-0.256	0.296	0.277	0.215
Z	-0.053	-0.453	0.050	-0.050	-0.165	-0.569	-0.065	-0.182	-0.926
A0	0.443	0.159	0.096	0.381	0.205	0.203	-1.850	0.143	0.084
TY	-0.039	-0.079	-0.088	-0.086	-0.090	-0.186	-0.131	-0.224	-13.414
S	-0.025	-0.074	0.259	-0.044	-0.134	0.731	-0.174	-0.328	0.273

Table 3. Diagonal components m^*_{ii} of the effective mass tensor m^*_{ij} for bottom CB of $In_xTl_{1-x}I$ crystals, calculated at selected *K*-points of BZ of primitive unit cells: C0 – -0.285,0.714,0; Z – 0,0,0.5; A0 – 0.285,0.285,0.5; TY - -0.5,0.5,0.2727; S – 0,0.5,0 (see Fig. 3)

CB	$x = 1.0$			$x = 0.50$			$x = 0$		
	m^*_{11}	m^*_{22}	m^*_{33}	m^*_{11}	m^*_{22}	m^*_{33}	m^*_{11}	m^*_{22}	m^*_{33}
C0	1.372	0.431	0.067	0.378	0.112	0.032	0.357	0.101	0.037
Z	-0.042	0.176	0.075	0.291	0.264	0.066	-0.131	0.576	0.070
A0	-0.023	-0.909	-1.135	-0.023	-0.673	-2.505	-0.020	-0.695	0.707
TY	0.193	0.063	0.034	0.176	0.073	0.057	1.394	0.645	0.091
S	-0.410	0.121	0.028	-0.418	0.112	0.039	-0.407	0.102	0.052

When the supercell 2×2×2 of the non-defective $In_{0.5}Tl_{0.5}I$ SSS crystal was used, the direct energy band gap $E_g = 1.332$ eV has been found to be at the BZ point 0,1/3,0 (Fig. 4a). This value of E_g is a bit larger in comparison to that ($E_g = 1.315$ eV) found for the primitive unit cell (Fig. 3). These differences may be due to the inclusion of interactions between more distant atoms in the supercell 2×2×2 in comparison to the primitive one.

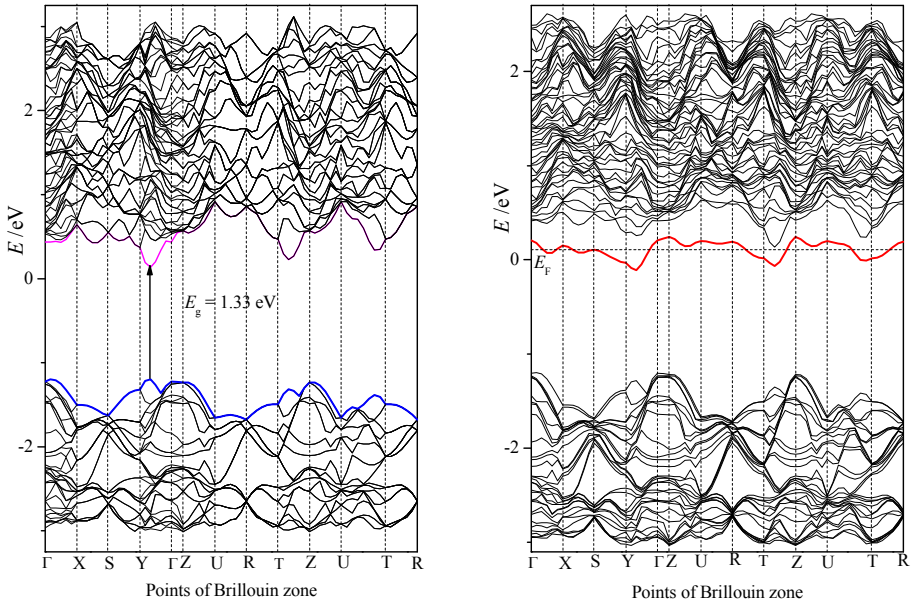

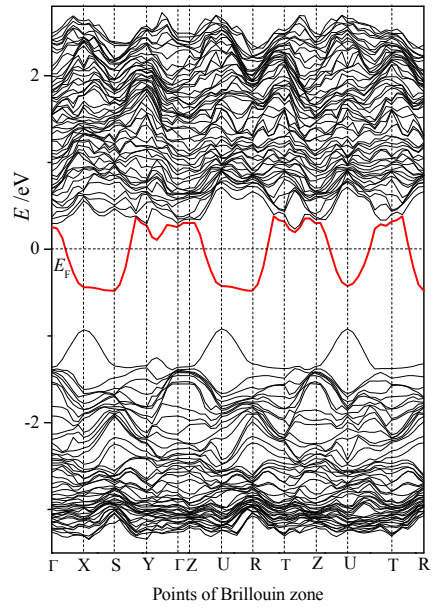

c)

Fig. 4. Band structures of (a) $In_{16}Tl_{16}I_{32}$ crystal (the space group of symmetry No. 38, *Amm*2), (b) $In_{16}Tl_{16}I_{31}$ (the space group of symmetry No. 25, *Pmm*2) with one iodine vacancy of the type I1 (see Fig. 1) and (c) $In_{16}Tl_{17}I_{32}$ crystal with one interstitial thallium atom (the space group of symmetry No. 25, *Pmm*2). Top VB and bottom CB are indicated at (a) in blue and magenta. The top half-occupied VBs are indicated in (b) and (c) by thick red lines and the Fermi level E_F by horizontal dashed lines. The set of BZ points Γ - 0,0,0; X - 1/2,0,0; S - 1/2,1/2,0; Y - 0,1/2,0; Z - 0,0,1/2; U - 1/2,0,1/2; R - 1/2,1/2,1/2; T - 0,1/2,1/2 corresponds to the space group of symmetry No. 25 (*Pmm*2)

On the basis of the crystal $In_{16}Tl_{16}I_{32}$ described above three defective crystals, the first, $In_{16}Tl_{16}I_{31}$, with iodine vacancy close to thallium atom, the second, $In_{16}Tl_{16}I_{31}$, with iodine vacancy close to indium atom, and the third, $In_{16}Tl_{17}I_{32}$, with interstitial thallium atom have been studied. Band structure of the crystal $In_{16}Tl_{16}I_{31}$ with vacancy defect (Fig. 4b) is similar to that of the non-defected one $In_{16}Tl_{16}I_{32}$ (Fig. 4a). One of the main differences is the larger number of energy bands in the case of $In_{16}Tl_{16}I_{31}$ (Fig. 4b) comparing to $In_{16}Tl_{16}I_{32}$ (Fig. 4a). The above feature may be caused by cancelation of the energy levels degeneracy due to the lower crystal symmetry of $In_{16}Tl_{16}I_{31}$ (space group No. 25) when compare to $In_{16}Tl_{16}I_{32}$ (space group No. 38). The other main difference is a position of the highest occupied energy band, which, in the defective crystal $In_{16}Tl_{16}I_{31}$, is located close to the unoccupied levels of the conduction band (Fig. 4b). The direct energy gap between

half-occupied and unoccupied bands, $\Delta E_{vc} \approx 0.2$ eV, may be, however, not sufficiently small to ensure the electron conductivity of the reasonable value at ambient temperature. An analysis of the partial density of states (PDOS) near the Fermi level E_F has revealed a high degree of the indium and thallium *p*-states hybridization at this half-occupied energy band. These *p*-states of indium and thallium form in predominant degree the top half-occupied band near Fermi level E_F. The contribution of the iodine *p*-states here is relatively smaller (Fig. 5a).

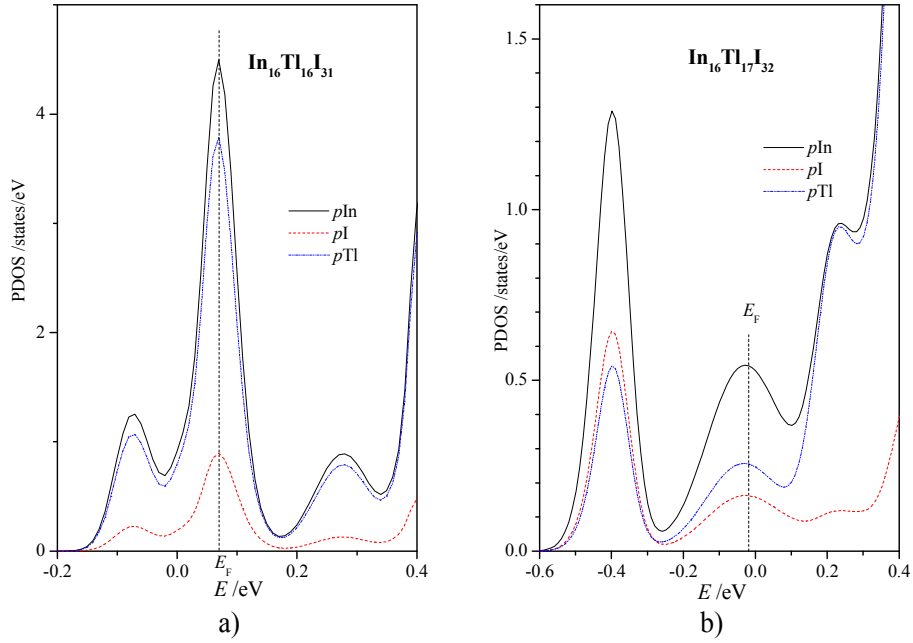

Fig. 5. Partial densities of (a) *p*-states of $In_{16}Tl_{16}I_{31}$ crystal with one iodine vacancy of the type I1 and (b) *p*-states of $In_{16}Tl_{17}I_{32}$ crystal with one interstitial thallium. The Fermi energy E_F is indicated by vertical dashed lines

Because of the large dimensions of thallium atom and the interstitial character of the corresponding defect the interatomic distances of Tl17 atom to the surrounding iodine and indium ones are smaller than the analogous values in the non-defective crystal $In_{16}Tl_{16}I_{32}$. In the present study, the interstitial Tl17 atom has been placed at the most symmetrical position with the nearest neighboring three iodine and two indium atoms. In this case, the symmetry of the optimized $In_{16}Tl_{17}I_{32}$ belongs to the space group No. 25 and is lower than that for the non-defective $In_{16}Tl_{16}I_{32}$ crystal (space group No. 38). In the relaxed crystal structure of $In_{16}Tl_{17}I_{32}$, the interatomic distances of interstitial thallium atom (Tl17) to the five nearest neighbors are the following: 3.089, 3.089 and 3.117 Å for Tl17 - I and 3.152 Å for

two Tl17 – In bonds. The absolute vales of Hirshfeld charges for Tl17 and these neighboring five ions are much smaller ($q_{Tl17} = 0.02$, $q_I = -0.09$, $q_{In} = 0.05$) than the similar charges of such ions located far from the interstitial defect ($q_{Tl} = 0.14$, $q_I = -0.13$, $q_{In} = 0.12$). This leads to the conclusion that the ionic type bonding of thallium atom with the above mentioned three iodine ones is much weaker in comparison to that between thallium and iodine atoms located far from the interstitial defect associated with Tl17 atom.

The Fermi energy E_F of $In_{16}Tl_{17}I_{32}$ corresponds to the averaged energy of the top half-occupied valence band, which is shown in Fig. 4c by thick red line. The dispersion of this energy band, $\Delta E \approx 0.9$ eV, is larger than the similar value for the case of $In_{16}Tl_{16}I_{31}$ crystal with one iodine vacancy (Fig. 4b). Upper parts of this half-occupied band are located very close ($\Delta E_{vc} \approx 0.02$ eV) to the more higher lying conduction bands (Fig. 4c). Due to this feature of the top half-occupied valence band one may expect increased electron conductivity associated with the unoccupied conduction bands of $In_{16}Tl_{17}I_{32}$ crystal in comparison to $In_{16}Tl_{16}I_{31}$ one with one iodine vacancy (Fig. 4b), where the similar binding energy is much larger ($\Delta E_{vc} \approx 0.2$ eV).

An analysis of PDOS near the Fermi level E_F (Fig. 5b) indicates lower degree of the indium and thallium *p*-states hybridization in comparison to the case of iodine vacancy (Fig. 5a). This is in agreement with much smaller Hirshfeld charge of the interstitial thallium ion, $q_{Tl17} = 0.02$, in comparison to that of the main matrix of $In_{16}Tl_{17}I_{32}$ crystal ($q_{Tl} = 0.14$). Thus, the interstitial thallium ion of $In_{16}Tl_{17}I_{32}$ participates not so much in the formation of the half-occupied top VB (Fig. 5b) in comparison to the formation of similar top VB in $In_{16}Tl_{16}I_{31}$ crystal with iodine vacancy (Fig. 5a). These results suggests the conclusion that the main reason for the half-occupied band formation near Fermi level may be the local distortion of crystal structure but not the deviations from the stoichiometric content of the chemical elements itself forming the nominal structure of a crystal.

For the defective crystals $In_{16}Tl_{16}I_{31}$ and $In_{16}Tl_{17}I_{32}$ the Fermi level E_F is shifted to the bottom conduction bands in comparison to the non-defective one (Fig. 4), that means an appearance of the donor states with the odd number of electrons in the top VB. As a result, the increased electron conductivity is expected in the defective crystals $In_{16}Tl_{16}I_{31}$ and $In_{16}Tl_{17}I_{32}$, caused by the intra- and inter-band electron transitions. In viewpoint of the relation between conductivity σ and dielectric permittivity ε,

$$\sigma = \sigma_1 + i\sigma_2 = -i\frac{\nu}{2}(\varepsilon_1 + i\varepsilon_2 - 1) \tag{2}$$

the spectral features of the imaginary part of dielectric function $\varepsilon_2(h\nu)$ at small photon energies are expected to be more pronounced than those for the real part of conductivity $\sigma_1(h\nu)$. In the case of defective crystals $In_{16}Tl_{16}I_{31}$ and $In_{16}Tl_{17}I_{32}$, the

total dielectric function $\varepsilon(h\nu)$ is a sum of two components corresponding to the inter- and intra-band electron transitions,

$$\varepsilon(h\nu) = \varepsilon_{inter}(h\nu) + \varepsilon_{intra}(h\nu) \quad (3)$$

Here, the intra-band component $\varepsilon_{intra}(h\nu)$ is usually associated with the low frequency and stationary electron conductivity, which is observed in metals and heavily doped semiconductors and is described satisfactorily by the monotonous Drude frequency dependence [30].

In view of the further discussion of the defective $In_{0.5}Tl_{0.5}I_{0.5}$ SSS we have approximated the CASTEP-calculated dielectric function $\varepsilon(h\nu)$ of the non-defective and defective SSS, taking into consideration the inter- and intra-band electron transitions using the OptaDOS code [31]. The intra-band part of dielectric function $\varepsilon_{intra}(h\nu)$ was approximated by the following relation according to the Drude model [28],

$$\varepsilon_{\text{intra}}(\nu) = 1 - \frac{\nu_p^2}{\nu^2 + i\gamma\nu} \quad (4)$$

where the constant value of broadening $\gamma = 10^{14}$ s^{-1} was used. The larger the plasmon frequency ν_p, the larger the imaginary part of dielectric function ε_{2intra} at the frequency $\nu = 0$, and the larger the expected direct (stationary) electron current conductivity $\sigma_{1intra}(0)$.

The polarized imaginary parts of dielectric functions $\varepsilon_2(h\nu)$ for the SSS studied are shown in Figs. 6 - 9. The main characteristic parameters of the crystals studied with 2×2×2 supercells, obtained using the OptaDOS code, are presented in Table 4. For the inter-band electron transitions, the dielectric function $\varepsilon_2(h\nu)$ of the non-defective $In_{16}Tl_{16}I_{32}$ reveals large anisotropy in the range of band gap, $h\nu \geq E_g = 1.33$ eV, which appears in the low energy shift of the dependence $\varepsilon_{2y}(h\nu)$ relating $\varepsilon_{2x}(h\nu)$ and $\varepsilon_{2z}(h\nu)$ ones (Fig. 6). This anisotropy of dielectric function is caused by the features of the top valence and bottom conduction bands of the crystal.

Analysis of dielectric functions of $In_{16}Tl_{16}I_{31}$ and $In_{16}Tl_{17}I_{32}$ crystals in the photon energy range about 0.4 – 1.8 eV (Figs. 7 - 9) with the corresponding band structures (Figs. 4b, 4c) permits to claim that the fine structure of $\varepsilon_2(h\nu)$ in this narrow range is formed by the electron transitions between the half-occupied top valence band and the lowest conduction bands. In turn the low-energy unstructured tail of the dependence $\varepsilon_2(h\nu)$ in the range 0 – 0.4 eV is formed due to the intra-band electron transitions within this half-occupied top valence band.

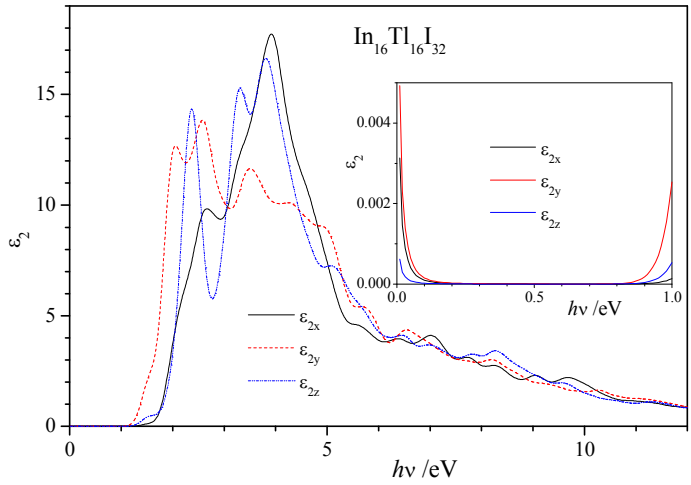

Fig. 6. Dielectric function $\varepsilon_2(h\nu)$ of $In_{16}Tl_{16}I_{32}$ crystal. ε_{2x} and ε_{2z} components correspond to the shortest (*a*) and longest (*b*) supercell dimensions (a = 9.527 Å, b = 9.575 Å, c = 25.193 Å). In the inset, the dependence $\varepsilon_2(h\nu)$ in the range 0 – 1.0 eV

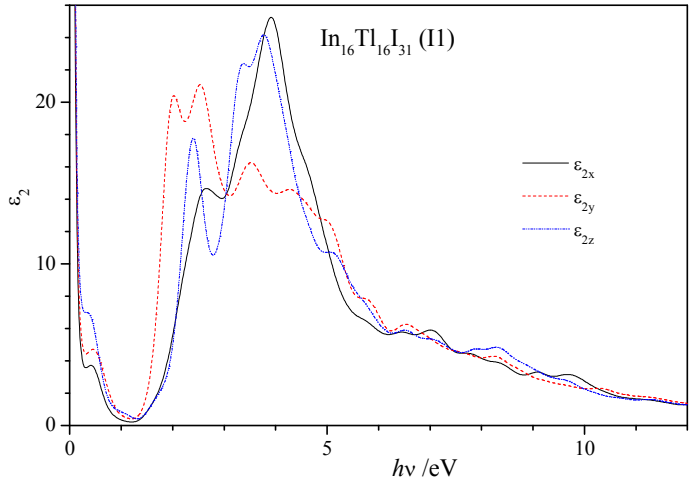

Fig. 7. Dielectric function $\varepsilon_2(h\nu)$ of $In_{16}Tl_{16}I_{31}$ with one iodine vacancy of the type I1 (see Fig. 1). ε_{2x} and ε_{2z} components correspond to the shortest (*a*) and longest (*c*) supercell dimensions (a = 9.517 Å, b = 9.518 Å, c = 25.185 Å)

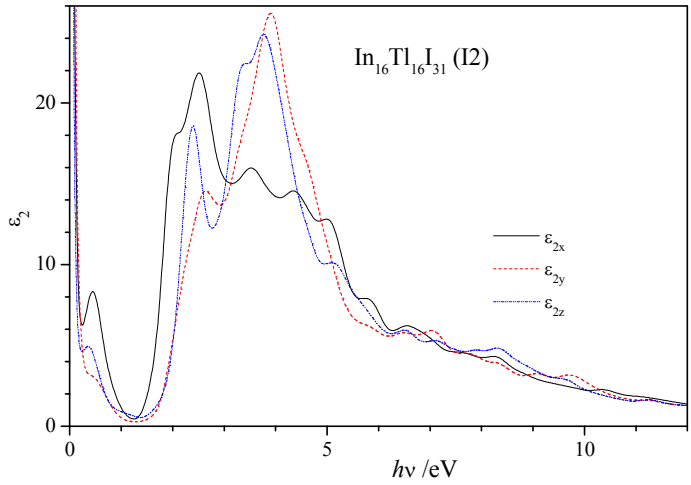

Fig. 8. Dielectric function $\varepsilon_2(h\nu)$ of $In_{16}Tl_{16}I_{31}$ with one iodine vacancy of the type I2 (see Fig. 1). ε_{2x} and ε_{2z} components correspond to the shortest (*a*) and longest (*c*) supercell dimensions (*a* = 9.466 Å, *b* = 9.540 Å, *c* = 25.266 Å)

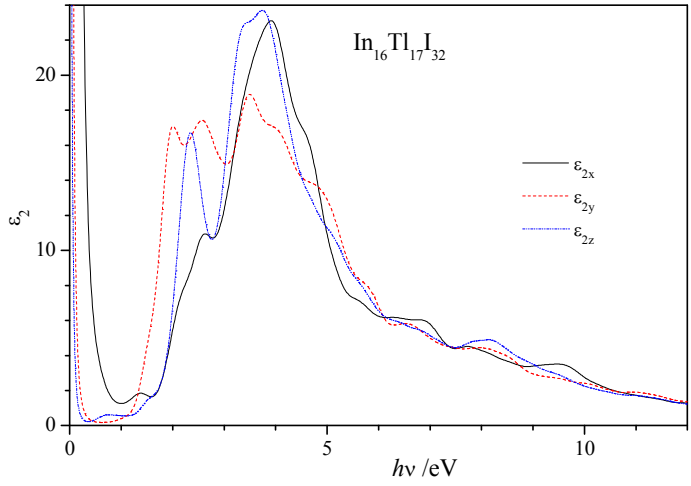

Fig. 9. Dielectric function $\varepsilon_2(h\nu)$ of $In_{16}Tl_{17}I_{32}$ crystal with one interstitial thallium atom. ε_{2x} and ε_{2z} components correspond to the shortest (*a*) and longest (*c*) supercell dimensions (*a* = 9.397 Å, *b* = 9.848 Å, *c* = 25.358 Å)

The iodine vacancies and thallium interstitials lead to the clear increase of the imaginary part of dielectric function $\varepsilon_2(h\nu)$ in the close vicinity of $h\nu = 0$ (Figs. 7 - 9). The largest increase of dielectric function $\varepsilon_2(h\nu)$ is observed for the case of thallium interstitial atom for the light polarization along *X*-axis (Fig. 9). For *Y*- and *Z*-polarizations the similar increase is much smaller (Fig. 9). Due to the features of the relation (3) the imaginary part of dielectric function $\varepsilon_2(h\nu)$ at the photon energy $h\nu$ close to zero is proportional to the plasmon frequency ν_p.

When comparing the plasmon energies ν_p for $In_{16}Tl_{17}I_{32}$ and $In_{16}Tl_{16}I_{31}$ (Table 4), the large spatial anisotropy in ν_p is observed for the crystal $In_{16}Tl_{17}I_{32}$ with thallium interstitial atom when compare to the relatively small one for $In_{16}Tl_{16}I_{31}$ crystals with iodine vacancy. For $In_{16}Tl_{17}I_{32}$ crystal this anisotropy correlates well with the corresponding energy vs. electron wave vector dispersion $E(\boldsymbol{K})$ of the top half-occupied band (Fig. 4c). For this top half-occupied band we have calculated the inverse electron mass tensor m^{*-1} at the *K*-points *X*, *S*, *U*, and *R* (Table 5) corresponding to the lowest band energies of the dispersion curve $E(K)$ (Fig. 4c). At these *K*-points, the mentioned band will rather be filled by the sole electron. The relation between three values $m^*_{\text{averaged}}{}^{-1}$ polarized along three Cartesian directions, $m^*_{\text{averaged}}{}^{-1}(100) > m^*_{\text{averaged}}{}^{-1}(010) > m^*_{\text{averaged}}{}^{-1}(001)$ (Table 5), is similar to the relation between three corresponding plasmon frequencies $\nu_p(100) > \nu_p(010) > \nu_p(001)$ (Table 4). This demonstrates that anisotropy of the dielectric function $\varepsilon_2(h\nu \to 0)$, the plasmon frequency ν_p and conductivity $\sigma_1(h\nu \to 0)$ for the intra-band electron transitions is closely related with anisotropy of the inverse electron mass $m^*_{\text{averaged}}{}^{-1}$ for the corresponding half-occupied band and BZ points at the lowest band energies. This conclusion is expected if one takes into account the known direct proportionality of the electron mobility μ and the inverse effective electron mass m^{*-1} [32, 33].

Table 4. Parameters related to the inter- and intra-band electron transitions in non-defective ($In_{16}Tl_{16}I_{32}$) and defective ($In_{16}Tl_{17}I_{32}$, $In_{16}Tl_{16}I_{31}$ (I1), $In_{16}Tl_{16}I_{31}$ (I2)) SSS calculated using OptaDOS code [31]

Parameter Crystal	Light polarization vector	Plasmon energy $h\nu_p$ /eV	Indirect band gap E_{gi} /eV	Direct band gap E_{gd} /eV	DOS at E_F (spin up ↑) DOS at E_F (spin down ↓)
$In_{16}Tl_{16}I_{32}$	(1 0 0)	$1.45\cdot10^{-3}$	1.531	1.54	$1.3\cdot10^{-5}$
	(0 1 0)	$1.82\cdot10^{-3}$			
	(0 0 1)	$6.43\cdot10^{-4}$			

$In_{16}Tl_{17}I_{32}$	(1 0 0)	1.66	0.054	0.53 (↑)	1.08 (↑)
	(0 1 0)	0.308		0.52 (↓)	1.08 (↓)
	(0 0 1)	0.173			
$In_{16}Tl_{16}I_{31}$	(1 0 0)	0.444	0.011	0.32 (↑)	2.79 (↑)
(I1 vacancy)	(0 1 0)	0.486		0.28 (↓)	2.61 (↓)
	(0 0 1)	0.497			
$In_{16}Tl_{16}I_{31}$	(1 0 0)	0.420	0.009	0.31 (↑)	2.65 (↑)
(I2 vacancy)	(0 1 0)	0.526		0.32 (↓)	2.61 (↓)
	(0 0 1)	0.311			

Table 5. Principal components of the inverse electron masses m^{*-1} for three Cartesian directions of the top half-occupied band of $In_{16}Tl_{17}I_{32}$ crystal calculated at four BZ points and the averaged one $m^{*}_{\text{averaged}}{}^{-1}$

	m^{*-1}/m_e		
Cartesian direction	100	010	001
BZ point			
X (0.5,0,0)	3.74	-0.241	0.473
S (0.5,0.5,0)	6.236	0.245	0.044
U (0.5,0,0.5)	4.122	-0.280	-0.446
R (0.5,0.5,0.5)	6.248	0.35	-0.039
$m^{*}_{\text{averaged}}{}^{-1}/m_e$	5.086	0.0185	0.008

Conclusion

DFT-based calculations of the band electronic structure and dielectric function have been performed for both the non-defective and defective (with iodine anion vacancy and thallium cation interstitial) solid state solutions of $In_{0.5}Tl_{0.5}I$. On the basis of the band structures obtained the tensors of effective electron mass have been calculated for the non-defective InI, $In_{0.5}Tl_{0.5}I$ and TlI crystals. Absolute values of the effective electron masses for the non-defective crystals studied have been found to be of the same order of magnitude. Minor decrease of the averaged effective electron masses takes place in the direction $TlI \rightarrow In_{0.5}Tl_{0.5}I \rightarrow InI$.

Imaginary part of the dielectric functions calculated for the defective solid state solutions of $In_{0.5}Tl_{0.5}I$ with taking into consideration the inter- and intra-band

electron transitions possesses the considerable, in comparison to the non-defective $In_{0.5}Tl_{0.5}I$ SSS, low-frequency component ($h\nu < 0.4$ eV). That points to the large low-frequency and stationary electron conductivity in the defective $In_{0.5}Tl_{0.5}I$ crystals. This finding is related to the crucial changes of band structure (formation of the donor half-occupied band close to the unoccupied conduction bands) due to the corresponding defects of SSS crystal structure (iodine vacancy or thallium interstitial atom). By taking into account defects in the calculation the results obtained are in qualitative agreement with experimental observations related to the band gap as well as *n*-type conductivity in $In_xTl_{1-x}I$ SSS [11]. Finally, it should be emphasized that in the case of real crystals, in particular metal-halides, in order to better match the calculated and experimental data, the existing structural imperfections should be taken into account in a suitable manner at the corresponding *ab initio* quantum chemical calculations.

Acknowledgments

Computer calculations have been performed using the Academic release of the CASTEP code (ver. 18.1) at WCSS of Wrocław University of Technology, Poland (project No. 053). The work was supported by the Project of Young Scientists (Co-66Hp) of Ukraine.

References

1. M.G. Kanatzidis, Discovery-synthesis, design, and prediction of chalcogenide phases. *Inorg. Chem.* 56 (2017) 3158 - 3173.
2. I. Chung, G. Mercouri, M.G. Kanatzidis, Metal chalcogenides: a rich source of nonlinear optical materials, *Chem. Mater.* 26 (2014) 849 - 869.
3. M. Piasecki, M.G. Brik, I.E. Barchiy, K. Ozga, I.V. Kityk, A.M. Al-Naggar, A.A. Albassam, T.A. Malakhovskaya, G. Lakshminarayana, Band structure, electronic and optical features of Tl_4SnX_3 (X=S, Te) ternary compounds for optoelectronic applications, *J. Alloy. Compd.* 710 (2017) 600-607. https://doi:10.1016/j.jallcom.2017.03.280.
4. Piasecki, M., Myronchuk, G.L., Zamurueva, O.V., Khyzhun, O.Y., Parasyuk, O.V., Fedorchuk, A.O., Albassam, A., El-Naggar, A.M., Kityk, I.V., 02/2016. Huge operation by energy gap of novel narrow band gap $Tl_{1-x}In_{1-x}B_xSe_2$ (B = Si, Ge): DFT, x-ray emission and photoconductivity studies. *Mater. Res. Express*, 3(2):025902. https://doi:10.1088/2053-1591/3/2/025902.
5. Brik, M.G., Piasecki, M., Kityk, I.V., Structural, Electronic, and Optical Features of $CuAl(S_{1-x}Se_x)_2$ Solar Cell Materials, 02/2014. *Inorg. Chem.*, 53:2645. https://doi:10.1021/ic403030w.

6. Atuchin V.V., et al., Structure, defects, mechanical and optical properties of hexagonal semiconductor $GaSe_{1-x}S_x$ single crystals, *Siberian Conference on Control and Communications*, Tomsk, IEEE Xplore 2007, pp. 179-184. https://doi: 10.1109/SIBCON.2007.371321.
7. Q. Guo, A. Assoud, H. Kleinke, Thallium-based chalcogenides as thermoelectrics, chapter 12, ed. C. Uher, Materials Aspect of Thermoelectricity, Boca Raton, CRC Press, 2016.
8. I.V. Blonsky, M.I. Kolinko, Yu.O. Lun, A.V. Franiv, Influence of static lattice disordering on optical properties of $In_xTl_{1-x}I$ crystals, *Proc. SPIE* 2647 (1995) 452-454. https://doi: 10.1117/12.226732.
9. A. Franiv, R. Peleshchyshyn, Y. Kolosivski, Optical properties of quantum size nanocrystals $In_xTl_{1-x}I$ embedded in solid matrices, *Ukr. J. Phys. Opt.* 1 (2000) 24-27. https://doi: 10.3116/16091833/1/1/24/2000.
10. Y.O. Dovhyi, A.V. Franiv, S.V. Ternavska, Isostructural phase transition in $In_xTl_{1-x}I$ system, *Ukr. J. Phys. Opt.* 2 (2001) 141-147. https://doi: 10.3116/16091833/2/3/141/2001.
11. A.I. Kashuba, M. Piasecki, O.V. Bovgyra, V.Yo. Stadnyk, P. Demchenko, A. Fedorchuk, A.V. Franiv, B. Andriyevsky, Specific features of content dependences for energy gap in $In_xTl_{1-x}I$ solid state crystalline alloys, *Acta Phys. Pol. A* 133 (2018) 68-75. https://doi: 10.12693/APhysPolA.133.68.
12. M.S. Brodin, I.V. Blonskii, B.M. Nitsovich, A.S. Krochuk, A.V. Franiv, Dynamical properties of excitons in layer crystals of PbI_2, *Phys. Status Solidi B* 111 (1982) 625-630. https://doi: 10.1002/pssb.2221110226.
13. R. Zallen, M.L. Slade, Inter-polytype conversion and layer-layer coupling in PbI_2, *Solid State Commun*. 17 (1975) 1561-1566. https://doi: 10.1016/0038-1098(75)90996-5.
14. A.V. Franiv, A.I. Kashuba, O.V. Bovgyra, Non-linear transducer of medium-infrared radiation, *Patent of Ukraine*, Bulletin No. 16, published on 2017-08-28 (http://base.uipv.org/searchINV/ , application number u201702658).
15. L. Helmholz, *Z. Kristallogr.* 95 (1936) 129-137.
16. R.E. Jones, D.H. Templeton, *The crystal structure of indium (I) iodide*, *Acta Crystallogr.* 8 (1955) 847. https://doi.org/10.1107/S0365110X55002594.
17. G. Meyer, T. Staffel, Note on the red monohalides of indium, InCl, InBr, InI, *Z. Anorg. Allg. Chem.* 574 (1989) 114-118. https://doi: 10.1002/zaac.655740112.
18. R.P. Lowndes, C.H. Perry, Molecular structure and anharmonicity in thallium iodide, *J. Chem. Phys.* 58 (1973) 271-278. https://doi: 10.1063/1.1678917.
19. A.V. Franiv, V.Y. Stadnyk, A.I. Kashuba, R.S. Brezvin, O.V. Bovgira, A.V. Futei, Temperature behavior of thermal expansion and birefringence of

$In_xTl_{1-x}I$ - substitution solid solutions, *Opt. Spectrosc.* 123 (2017) 177-180. https://doi: 10.1134/S0030400X17070074.

20. A.V. Franiv, A.I. Kashuba, O.V. Bovgyra, O.V. Futey, Elastic properties of substitutional solid solutions $In_xTl_{1-x}I$ and sounds wave velocities in them, *Ukr. J. Phys.* 62 (2017) 679-684. https://doi: 10.15407/ujpe62.08.0679.
21. A.I. Kashuba, A.V. Franiv, R.S. Brezvin, O.V. Bovgyra, Birefringence of $In_xTl_{1-x}I$ solid state solution, *Functional materials* 23 (2017) 26–30. https://doi: 10.15407/fm24.01.026.
22. A.I. Kashuba, Ya.A. Zhydachevskyy, I.V. Semkiv, A.V. Franiv, O.S. Kushnir, Photoluminescence in the solid solution $In_{0.5}Tl_{0.5}I$, *Ukr. J. Phys. Opt.* 19 (2018) 1-8.
23. S.J. Clark, M.D. Segall, C.J. Pickard, P.J. Hasnip, M.J. Probert, K. Refson, M.C. Payne, First principles methods using CASTEP, *Zeitschrift für Kristallographie* 220 (2005) 567-570. https://doi: 10.1524/zkri.220.5.567.65075.
24. Perdew, J.P., Ruzsinszky, A., Csonka, G.I., Vydrov, O.A., Scuseria, G.E., Constantin, L.A., Zhou, X., Burke, K., Restoring the Density-Gradient Expansion for Exchange in Solids and Surfaces, 2008. *Phys. Rev. Lett.* 100, 136406. https://doi: 10.1103/PhysRevLett.101.239702.
25. H.J. Monkhorst, J.D. Pack, Special points for Brillouin-zone integrations, *Phys. Rev.* B13 (1976) 5188-5192. https://doi.org/10.1103/PhysRevB.13.5188.
26. Y. Hinuma, G. Pizzi, Y. Kumagai, F. Oba, I. Tanaka, Band structure diagram paths based on crystallography, *Comp. Mater. Sci.* 128 (2017) 140-184. https://doi: 10.1016/j.commatsci.2016.10.015.
27. L. Pauling, *The Nature of the Chemical Bond,* 3rd edition. Copyright 1939 and 1940, 3rd edition copyright © by Cornell University, 1960.
28. M. Grundmann. *The Physics of Semiconductors*, Springer-Verlag Berlin Heidelberg, 2006.
29. Fonari, A., Sutton, C., Effective mass calculator, 2012.
30. H. Fujiwara, *Spectroscopic ellipsometry: principles and applications*, John Wiley & Sons Ltd, The Atrium, Southern Gate, Chichester, 2007.
31. A.J. Morris, R. Nicholls, C.J. Pickard, J. Yates, OptaDOS: A tool for obtaining density of states, core-level and optical spectra from electronic structure codes, *Comp. Phys. Comm.* 185 (2014) 1477-1485. https://doi: 10.1016/j.cpc.2014.02.013.
32. P.Y. Yu, M. Cardona, *Fundamentals of Semiconductors: Physics and Materials Properties*. Springer, 2010.

33. Hou, Q.Y., Li, W.C., Xu, Z.C., Zhao, C.W., Study on the effect of high V doping on the conductivity of anatase TiO_2, 2016. *Int. J. Modern Phys. B* 30, 165001. https://doi: 10.1142/S0217979216500016.

Abstract

We investigate an influence of the various crystal structure imperfections on the electronic properties and dielectric functions for $In_{0.5}Tl_{0.5}I$ semiconductor in the frame of the density functional theory calculations. The tensor of electron effective mass m^*_{ij} of InI, $In_{0.5}Tl_{0.5}I$ and TlI crystals has been calculated for the valence and conduction bands and different *K*-points of Brillouin zone. Dielectric functions $\varepsilon(h\nu)$ of the defective crystals based on $In_{0.5}Tl_{0.5}I$ solid state solution with iodine vacancy and thallium interstitial atom were calculated taking into consideration the inter-band and intra-band electron transitions. The studies of the defective crystals reveal increased low-frequency and stationary electron conductivity with anisotropy resulted from the anisotropy of the electron effective mass tensor. Our findings explain the origin of crucial changes in the band structure by formation the donor half-occupied levels close to the unoccupied conduction bands due to the crystal structure defects, i.e. iodine vacancy or thallium interstitial atom. It has been shown that in the case of real crystals, in particular metal-halides, the proper consideration of defects in quantum-chemical calculations results in a better matching of the theoretical and experimental results in comparison to the case when the perfect crystal structure had been used for calculations.

Streszczenie

Zbadano wpływ różnych niedoskonałości struktury krystalicznej na właściwości elektronowe i funkcje dielektryczne półprzewodnika $In_{0.5}Tl_{0.5}I$ w ramach teorii funkcjonału gęstości. Został obliczony tensor efektywnej masy elektronów m^* kryształów InI, $In_{0.5}Tl_{0.5}I$ i TlI dla pasm walencyjnych i przewodnictwa oraz różnych K-punktów strefy Brillouina. Funkcje dielektryczne $\varepsilon(h\nu)$ domieszkowanych kryształów roztworów stałych $In_{0.5}Tl_{0.5}I$ z wakansami jodu i atomami międzywęzłowymi talu zostały obliczone z uwzględnieniem międzypasmowych i wewnątrz-pasmowych przejść elektronowych. Badania domieszkowanych kryształów ujawniły zwiększoną przewodność elektronową niskoczęstotliwościową i stacjonarną o anizotropii wynikającej z anizotropii tensora efektywnej masy elektronów. Przeprowadzone badania wyjaśniają obserwowane duże zmiany struktury pasmowej pochodzące z utworzenia pół wypełnionych poziomów donorowych w pobliżu niezajętych pasm przewodnictwa wynikających z defektów struktury krystalicznej, tj. wakansów jodu czy atomów międzywęzłową talu. Wykazano, że w przypadku kryształów rzeczywistych, w szczególności halogenków

metali, właściwe uwzględnienie defektów w obliczeniach kwantowo-chemicznych daje możliwość lepszego dopasowania obliczeń teoretycznych do wyników doświadczalnych w porównaniu do obliczeń bazujących na strukturze krystalicznej doskonałej.